The Shape Effect of Mesoporous Silica Nanoparticles on Biodistribution, Clearance, and Biocompatibility *in Vivo*

Xinglu Huang,[†,¶] Linlin Li,[†,¶] Tianlong Liu,[†] Nanjing Hao,[†,‡] Huiyu Liu,[†] Dong Chen,[†] and Fangqiong Tang[†,*]

[†]Laboratory of Controllable Preparation and Application of Nanomaterials, Technical Institute of Physics and Chemistry, Chinese Academy of Sciences (CAS), Beijing 100190, China and [‡]Graduate University of the Chinese Academy of Sciences, Beijing, 100049, China. [¶]These authors have equally contributed to the article.

ABSTRACT In our previous study we reported that the interaction of nanoparticles with cells can be influenced by particle shape, but until now the effect of particle shape on *in vivo* behavior remained poorly understood. In the present study, we control the fabrication of fluorescent mesoporous silica nanoparticles (MSNs) by varying the concentration of reaction reagents especially to design a series of shapes. Two different shaped fluorescent MSNs (aspect ratios, 1.5, 5) were specially designed, and the effects of particle shape on biodistribution, clearance and biocompatibility *in vivo* were investigated. Organ distributions show that intravenously administrated MSNs are mainly present in the liver, spleen and lung (>80%) and there is obvious particle shape effects on *in vivo* behaviors. Short-rod MSNs are easily trapped in the liver, while long-rod MSNs distribute in the spleen. MSNs with both aspect ratios have a higher content in the lung after PEG modification. We also found MSNs are mainly excreted by urine and feces, and the clearance rate of MSNs is primarily dependent on the particle shape, where short-rod MSNs have a more rapid clearance rate than long-rod MSNs in both excretion routes. Hematology, serum biochemistry, and histopathology results indicate that MSNs would not cause significant toxicity *in vivo*, but there is potential induction of biliary excretion and glomerular filtration dysfunction. These findings may provide useful information for the design of nanoscale delivery systems and the environmental fate of nanoparticles.

KEYWORDS: mesoporous silica nanoparticles (MSNs) · shape · *in vivo* · biodistribution · clearance · biocompatibility

Nanoenabled drug delivery systems are gaining application in the pharmaceutical industry, since nanoparticle-based drugs may have improved solubility and altered pharmacokinetics and biodistributions compared to small molecule drugs.[1−3] The future success of nanoparticle-based nanomedicine requires nanoparticles (NPs) with well-defined *in vivo* behaviors. Elucidating the *in vivo* biodistribution, clearance, and biocompatibility of administered NPs, as important indications of *in vivo* behavior, is considered very important in the context of the underlying medical debate regarding the safety of novel nanodelivery systems. In view of the complexity of designed nanoplatforms, there are still many unanswered questions regarding their *in vivo* behaviors.

There is now ample evidence that physicochemical properties, such as size, shape, and surface chemistry, can dramatically influence the behaviors of NPs in biological systems and might, in part, determine the biodistribution, clearance, and biocompatibility of NPs *in vivo*. In this regard, some *in vitro*[4−9] and *in vivo*[10−14] studies have demonstrated the effect of size and surface chemistry of NPs on biological behaviors. For example, Jong *et al.*[15] demonstrated that tissue distribution of gold NPs is size-dependent with the smallest 10 nm NPs showing the most widespread organ distribution. He *et al.*[16] indicated that different surface-modified silica NPs (OH−, COOH−, and PEG−) are all cleared from the systemic blood circulation, but both the clearance time and subsequent biological organ deposition are dependent on the surface chemical modification of particles. Although some reports have shown that the shape of NPs plays an important role in biological effects *in vitro*,[17−19] there are very few reports on the effects of particle shape on *in vivo* biological behaviors,[20] even as interest on the design of high performance drug delivery systems grows. This may be due to the limited availability of techniques to produce nonspherical biocompatible NPs.[21] Most importantly, there are few particle fabrication techniques currently available which have the ability to independently alter one variable at a time and monitor the effect of each variable.

Mesoporous silica nanoparticles (MSNs) have recently attracted much attention in the biomedical field due to their unique characteristics, including high Brunauer, Emmet and Teller (BET) surface area, large pore volume, and uniform porosity, making them excellent candidates for the development of a drug delivery system.[22−24]

* Address correspondence to tangfq@mail.ipc.ac.cn.

Received for review January 29, 2011 and accepted June 2, 2011.

Published online June 02, 2011
10.1021/nn200365a

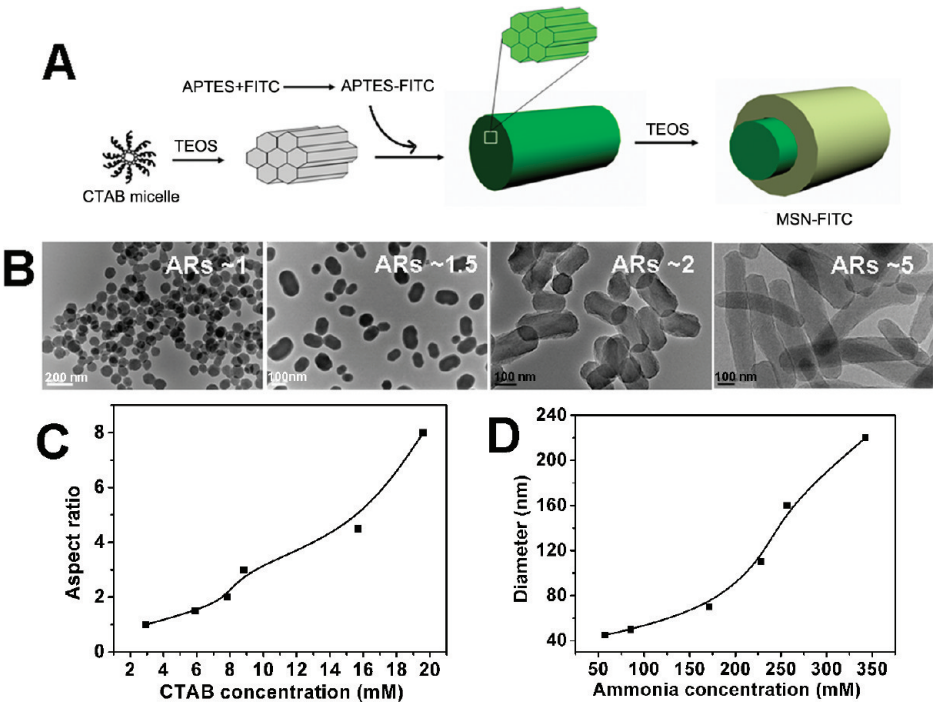

Figure 1. Controlled fabrication and characterization of MSN–FITC. (A) Illustration of the fabrication of MSN–FITC by a specifically designed two-step preparation. (B) TEM images of different shaped MSN–FITC. The shapes of particles were controlled by CTAB concentration. (C) Relationship of CTAB concentration and aspect ratios (ARs). (D) Relationship of aqueous ammonia concentration and diameters.

Previous reports indicated that some nonspherical MSNs show advantages in biomedical applications. For example, rodlike multifunctional MSNs display great potential in monitoring cell trafficking, cancer cell metastasis, and drug/DNA delivery.[25] In our previous studies, different shaped MSNs of similar particle diameter, chemical composition and surface charge but with different aspect ratios (ARs) were specially designed. The shape effect of MSNs on cellular uptake and behaviors was then illustrated.[26] To further investigate the shape effect on *in vivo* behaviors, different shaped fluorescent particles with fluorescein isothiocyanate (FITC) molecules doped in the mesoporous silica shells (MSN–FITC) was controllably fabricated in this study. Moreover, the functionalization of NPs by PEG chains is probably the most efficient way to avoid nonspecific accumulation that can be detrimental for the *in vivo* application of NPs.[13] So, we designed two rodlike shaped MSN–FITC (ARs 1.5, 5) and modified them with PEG molecules to track the biodistribution of particles *in vivo* after intravenous injection. To further quantitatively analyze the biodistribution and clearance of different shaped and PEGylated MSN–FITC, the Si content in blood and target organs was analyzed by inductively coupled plasma atomic emission spectroscopy (ICP–OES). Additionally, the biocompatibility of different shaped and PEGylated MSN–FITC was studied by the analysis of hematology, serum biochemistry, and histopathology.

RESULT AND DISCUSSION

Controlled Fabrication of MSN–FITC. MSN–FITC were synthesized in a specifically designed two-step preparation (Figure 1A). Briefly, 3-aminopropyl triethoxysilane–fluorescein isothiocyanate (APTES–FITC) solution was prepared by conjugating FITC with APTES. Separately, particles were synthesized by co-condensation of tetraethyl orthosilicate (TEOS) and FITC–APTES in the presence of aqueous ammonia and cetyltrimethylammonium bromide (CTAB). A two-step procedure needed to add TEOS during the synthesis process of MSN–FITC. First, two-third of TEOS was added to the mixture of CTAB and $NH_3 \cdot H_2O$ with vigorous stirring for 1 h and then APTES–FITC and additional TEOS was added. In this fabrication, the shape and size of MSN–FITC is controlled by changing the concentration of reaction reagents. The shape of particles is mainly dependent on CTAB concentration. The ARs of MSN–FITC were varied from ~1 to ~8 (Figure 1C) when the CTAB concentration increased from 2.94 mM to 19.6 mM. Furthermore, the concentration of aqueous ammonia plays an important role in the diameter of MSN–FITC. For example, ~70 nm MSN–FITC with ARs of ~1.5 were produced with reactant concentration of 5.9 mM CTAB, 171 mM $NH_3 \cdot H_2O$ and 41 mM TEOS, while ~160 nm MSN–FITC with ARs of ~1.5 were obtained by increasing the ammonia concentration to 256 mM (Figure 1D). The controlled synthesis of shape and diameter of MSNs provides the foundation for designing the needed MSNs to assess biological effects.

The fluorescent images of different shaped MSN–FITC and FITC solution were observed under UV excitation, and absorption and fluorescence spectra were also measured by a spectrometer (Supporting Information, Figure S1). The results indicate that the absorption spectra of FITC are different from that of MSN–FITC. The possible reason is that the molecular structure of FITC molecules is changed during conjugation with APTES, causing a red shift of the absorption peak. Importantly, the change in the absorption spectra did not influence the fluorescent property of MSN–FITC, which is still suitable as imaging probes. To obtain fluorescent NP probes, fluorescent dyes are generally labeled on the surface of NPs. However, this labeling strategy may be unsuitable for long-term tracking *in vivo* biodistribution of the particles. Two possible reasons are, first, fluorescent molecules coupled on the surface of NPs could detach from the particles which would alter the *in vivo* readouts; second, fluorescent molecules on the surface of NPs would be greatly affected by biofluids (i.e., pH environment, enzyme), easily causing fluorescent signal quenching. In order to create more robust probes, hybrid organic/inorganic NPs have been developed from organic dye molecules and silica.[27,28] As a matrix material for fluorescent probes, silica provides a chemically and mechanically stable vehicle, which can protect the encapsulated dye molecules from external perturbations, while exposing a biocompatible and easily functionalized surface to the environment and in some cases enhancing the photophysical properties of the encapsulated dyes.[29] Therefore, we designed and synthesized particles with FITC embedded into MSNs to prevent quenching and falloff of the dye molecules, which is suitable for long-term tracking of the particle biodistribution *in vivo*.

Design of different shaped and PEGylated MSN–FITC. In view of the above controlled fabrication, we designed two shaped MSN–FITC with similar particle diameters, chemical compositions and surface charges but with different ARs (1.5, 5) and then investigated the effect of particle shape on biodistribution, clearance and biocompatibility *in vivo*. First, the biodistribution of particles was observed by fluorescent images of MSN–FITC in the major organs of mice. Quantitative studies of MSN–FITC biodistribution and excretion were further performed by determination of Si content with ICP–OES analysis. Finally, we studied the biocompatibility of MSN–FITC including hematology, serum biochemistry and histopathology analysis.

To compare the shape effect of particles on biodistribution, clearance and biocompatibility, two kinds of shaped MSN–FITC with well-ordered hexagonal pore structures were synthesized. The TEM images show the short rod MSN–FITC (ARs of ~1.5, length of 185 nm ±22 nm) and long rod MSN–FITC (ARs of ~5, length of 720 nm ±65 nm) are both composed of two layer

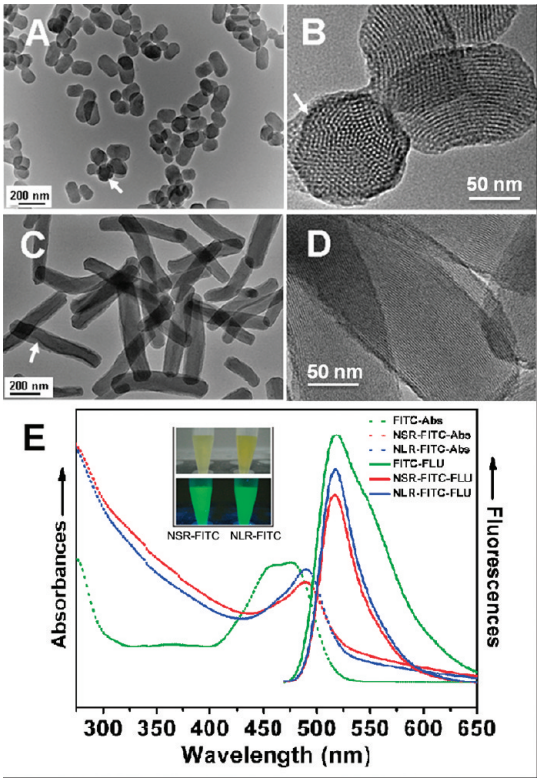

Figure 2. Characterization of NSR–FITC and NLR–FITC. (A) TEM image of NSR–FITC. (B) TEM image showing the mesostructure of NSR–FITC. (C) TEM image of NLR–FITC. (D) TEM image showing the mesostructure of NLR–FITC. (E) Absorption and emission spectra of FITC, NSR–FITC, and NLR–FITC. Arrow denotes FITC embedded into particle.

structures (Figure 2A–D, arrow). This is due to the two-step process used to add TEOS during the synthesis process, where the as-synthesized inner layer of MSN–FITC was embedded with FITC giving an obvious contrast. The fluorescent spectra of short rod MSN–FITC (NSR–FITC) and long rod MSN–FITC (NLR–FITC) indicate that their fluorescent properties were similar with FITC and suitable for fluorescent imaging (Figure 2E).

Previous researchers have demonstrated that PEGylation reduces the rate of mononuclear phagocyte system uptake and increases circulation half-life for various types of spherical NPs, including liposomes, polymer-based NPs, and hybrid NPs.[30] It has been hypothesized that PEG creates a steric shield around the coated particle, effectively preventing plasma proteins adhering to the particle surface and thus avoiding subsequent uptake by mononuclear phagocytes.[1] To research the effect of PEGylation on circulation time and biocompatibility of nonspherical MSN–FITC, PEG modification was performed by the conjugation strategy as described in the Experimental Section. The ζ potential changes of modified MSN–FITC indicate that the particle surfaces were successfully modified by APTES and PEG molecules, respectively (Supporting Information, Figure S2). The PEG packing density on MSN was estimated to be about 0.61 and 0.87 PEG

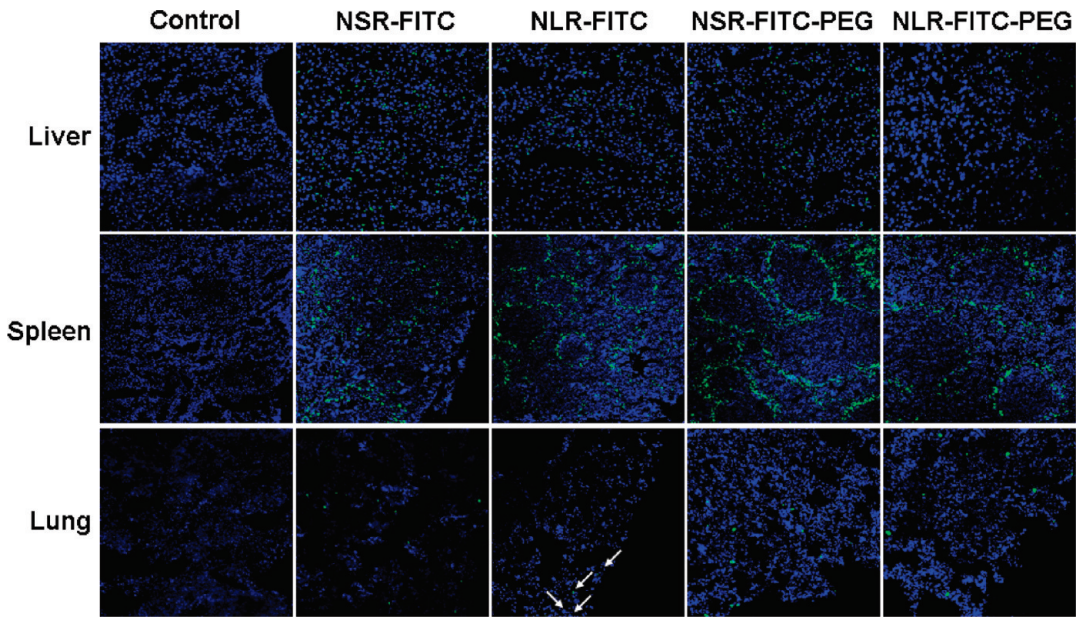

Figure 3. Biodistribution of different shaped and PEGylated MSN–FITC in liver, spleen, and lung was observed by confocal microscopy images 2 h after intravenous injection. Arrows denote NLR–FITC distribution in lung.

molecules per square nanometer surface area for NSR and NLR, respectively.[31,32]

Biodistribution of Different Shaped MSN–FITC and MSN–FITC-PEG *in Vivo*. To study the *in vivo* biodistribution of particles, organs of mice injected with either MSN–FITC or MSN–FITC-PEG were collected, and the frozen tissue sections were obtained by microtome. After DAPI ((2-(4-amidinophenyl)-6-indolecarbamidine dihydrochloride) staining, fluorescent images of the tissue sections were acquired by confocal microscopy. The results indicate that four kinds of particles (green) were mainly distributed in the liver, spleen, and lung 2 h after injection (Figure 3). They showed diffused distribution in the liver and lung and aggregated distribution in the marginal zone of the spleen. This punctuated particles distribution in tissues is related to the distribution of mononuclear phagocytes. We found there was weaker fluorescent signal intensity at 7 d postinjection than that at 2 and 24 h postinjection (data not shown). The possible reasons for this phenomenon is that the particle fluorescent signals are quenched in tissues after 7 d post-treatment or the silica particles are biodegraded or excreted from the body.[14] More detailed information of the particles in different tissues at different time points is shown in Supporting Information, Figures S4–S9. The MSN–FITC fluorescent signals in the organs were still present 7 d after injection, so it can be considered as a robust fluorescent probe for tracking the biodistribution of NPs. MSN–FITC serum stability was also studied and indicated it is a robust fluorescent probe (Supporting Information, Figure S3).

Many previous reports have indicated that NPs can reach specific sites for diagnosis and therapy of disease, such as the lymph nodes[33] and brain parenchyma across the blood-brain barriers.[34] After 2 h or 7 d postinjection, we did not find the presence of the four kinds of particles in the limb lymph nodes and brain (Figure S12 and 13), which indicated they did not spread into peripheral sites nor pass through the blood-brain barrier. The reason for this phenomenon may be related to the intrinsic properties of NPs, such as size[35] and surface chemistry.[36] Previous studies indicated silica nanoparticles could be partly excreted through the renal excretion route.[16] In this study, a little MSN–FITC and MSN–FITC–PEG were found in the kidney at 2 h postinjection, while only NSR–FITC–PEG and NLR–FITC–PEG were observed at the 7 d time point (Figure S10 and 11). This result demonstrates that naked and PEGylated MSNs may enter the kidney and pass through glomerular filtration, providing a potential metabolism route. These *in vivo* biodistribution results of MSNs are consistent with previous reports,[37,38] which indicate that the particles are mainly uptaken by reticuloendothelial system (RES).

Quantitative Analysis of Biodistribution and Clearance of Different Shaped and PEGylated MSN–FITC. To quantify the biodistribution, equivalent doses of different shaped and PEGylated MSNs were intravenously injected and Si content in blood and organs was measured with ICP–OES. Figure 4 shows the biodistribution in major organs and blood after 2 h, 24 h, and 7 d of administration. Different shaped and PEGylated MSNs were mainly trapped in RES of the liver, spleen, and lung, accounting for over 80% of the injected dose at 2 h after administration. There are obvious differences in the biodistribution trend for the different shaped and PEGylated MSNs as shown in Figure 4A. NSR were easily trapped in the liver, while more NLR distributed in the

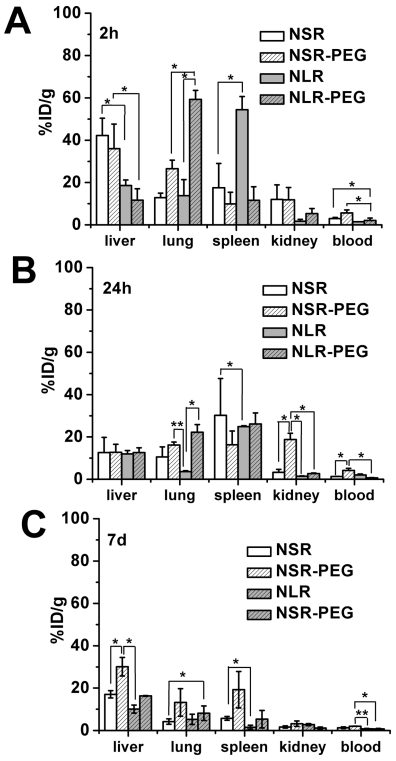

Figure 4. Quantitative analysis of different shaped and PEGylated MSNs in organs and blood by ICP−OES. Relative Si contents in liver, spleen, and kidney at (A) 2 h, (B) 24 h, and (C) 7 d postinjection. Data are the mean ± SD from three separate experiments. Asterisk (∗) or double asterisk (∗∗) denotes statistical significance for the comparison of Si contents of different shaped and PEGylated MSNs in organs and blood: ∗, $p < 0.05$; ∗∗, $p < 0.01$.

spleen ($p < 0.05$). After PEGylation, the liver capture of NSR was decreased ($p < 0.05$). It was surprising that the PEGylated NSR and NLR both had a higher content in the lung than the naked NPs ($p < 0.05$) and indicates that surface modification also changed the *in vivo* biodistribution of NPs.

Comparing the Si contents of organs at 2 h, 24 h, and 7 d postinjection, we found that the Si content of these organs were obviously decreased over time and indicated MSNs could be biodegraded or cleared from liver, spleen, lung, and kidney (Supporting Information, Figure S14). NLR (from 30% to 70% in different organs) had a faster clearance rate relative to NSR (from 10% to 20% in different organs), especially in spleen and lung ($p < 0.01$). PEG modification obviously decreased the clearance rate of MSNs in organs ($p < 0.05$), demonstrating that the PEGylated NPs were more difficult to be removed from the RES organs regardless of the particle shape. This result is inconsistent with a previous report that PEGylated single-walled carbon nanotubes (SWNTs) have a relatively fast clearance rate from organs[39] than naked SWNTs. This may be attributed to the hydrophobic properties of SWNTs, which may elongate the retention time of SWNTs *in vivo*.

In terms of the circulation time of particles in blood, the NLR and NSR did not show detectable concentration differences in blood at 2 h after administration. At 24 h, Si contents of NSR in blood significantly deceased ($p < 0.05$), while that of PEGylated NSR did not show obvious changes. In addition, we found the Si content of NLR at 24 h postadministration maintained a similar level as 2 h. After 7 d postadministration, all the Si content of these four kinds of MSNs decreased to a low level ($p < 0.05$). The results indicate NLR has a longer blood circulation time than NSR, while the effect of PEGylation on blood circulation time is partially dependent on the shape of the NPs.

From the above results, we found the shape and surface modification of NPs influence the *in vivo* biodistribution and retention ability in tissues. NP uptake by immune cells may occur both in the bloodstream by monocytes, platelets, leukocytes, and dendritic cells (DC) and in tissues by resident phagocytes (*e.g.*, Kupffer cells in liver, alveolar macrophages in lung, DC in lymph nodes, macrophages and B cells in spleen).[1] Therefore, the biodistribution and retention ability of particles in tissues may be relative to the uptake ability of these immune cells.

Excretion of Different Shaped and PEGylated MSNs *in Vivo*. It was observed that the injected MSNs can reach the kidney, so we further investigated whether MSNs could be excreted from the body and analyzed the effect of particle shape on excretion. The urine and feces samples were collected by metabolic cages at different time points after injection of MSNs, and the results were then determined by ICP−OES (Figure 5). Because the mice had free access to water and commercial laboratory complete food, the silicon content in the feces and urine of the control group were very high and fluctuating. It interfered with the calculation of excretion percentage. At 2 h postinjection, Si was detected in the urine for all the NPs (Figure 5A), and the excreted Si content of NSR was significantly higher than that of NLR ($p < 0.05$). The MSN excretion in urine corresponds to the biodistribution of MSNs in kidney and clearance rate of MSNs (Figures 3 and 4). At 2 h postinjection, Si content in feces for NSR was obviously higher than the control group but was not observed for other particles (Figure 5B). At 7 d, however, the particles exhibited an obvious feces excretion. The possible reason is that the excretion of NPs through feces is performed by hepatic processing and biliary excretion after liver uptake, which is relatively slower than the renal clearance route. Overall, MSNs can be excreted by urine and feces and NSRs have a more rapid clearance rate than NLRs in both routes. In view of the excretion differences between MSNs and PEGylated MSNs *in vivo*, we deduce particle surface charge, as shown in Supporting Information, Figure S2, plays an important role. A previous study discovered surface charge-mediated rapid hepatobiliary excretion of MSNs and indicated that the particles with more highly charged moieties (+34.4 mV) were quickly excreted from the

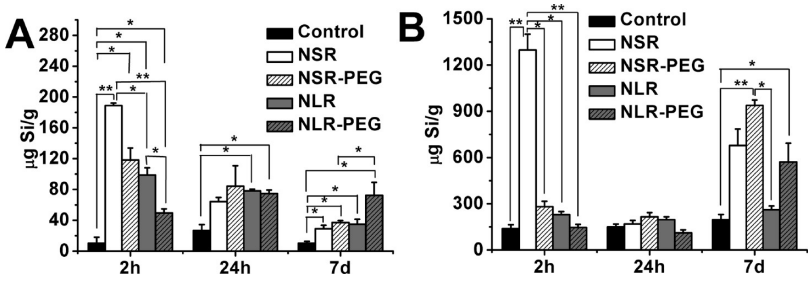

Figure 5. ICP−OES quantitative analysis of the Si content in (A) urine, and (B) feces at 2 h, 24 h, and 7 d after injection. Data are the mean ± SD from three separate experiments. Asterisk (∗) or double asterisk (∗∗) denotes statistical significance for the comparison of the Si contents of different shaped and PEGylated MSNs in urine and feces, ∗, $p < 0.05$; ∗∗, $p < 0.01$.

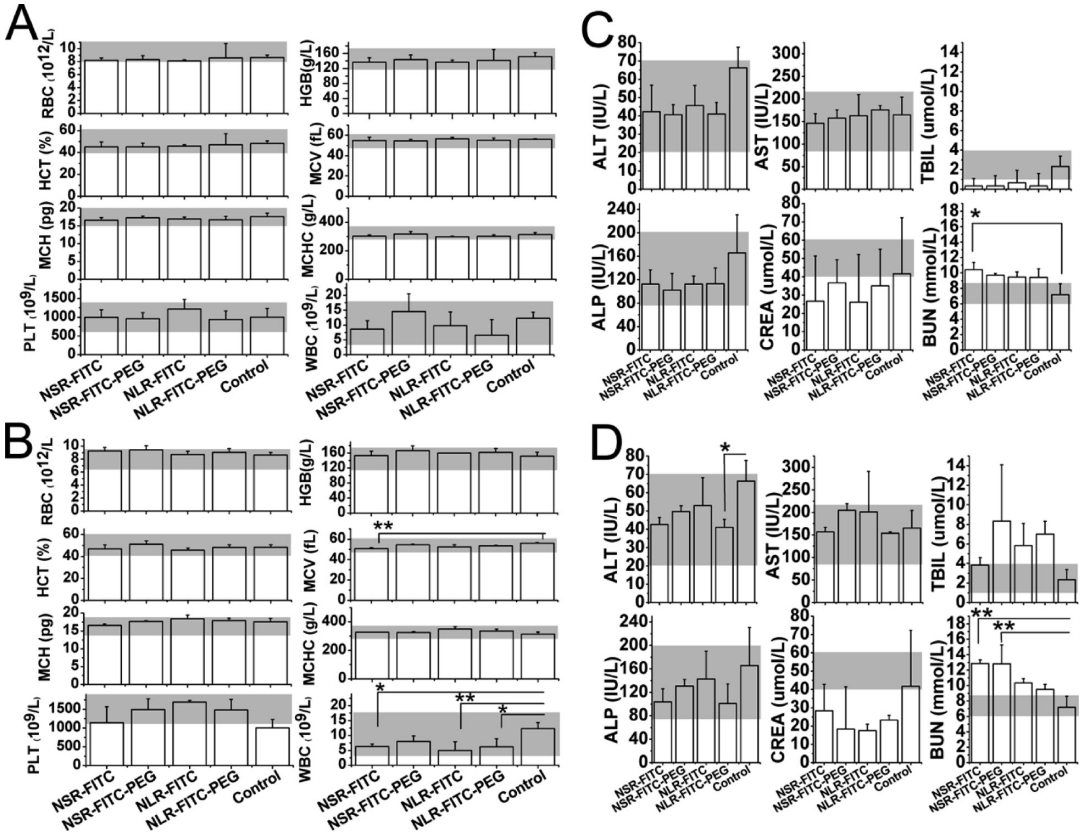

Figure 6. Effect of different shaped and PEGylated MSNs on (A,B) hematology and (C,D) serum biochemistry at (A,C) 24 h and (B,D) 18 d. Relative hematology indicators include red blood cell count (RBC), hemoglobin (HGB), hematocrit (HCT), mean corpuscular volume (MCV), mean corpuscular hemoglobin (MCH), mean corpuscular hemoglobin concentration (MCHC), platelet count (PLT) and white blood cell count (WBC). Related serum biochemistry indicators include alanine aminotransferase (ALT), aspartate aminotransferase (AST), total bilirubin (TBIL), alkaline phosphatase (ALP), creatinine (CREA), and blood urea nitrogen (BUN). Data are the mean ± SD from three separate experiments. Asterisk (∗) or double asterisk (∗∗) denotes statistical significance for the comparison of the effect of different shaped and PEGylated MSNs on hematology and serum biochemistry: ∗, $p < 0.05$; ∗∗, $p < 0.01$. Gray bars indicate the range of values obtained from healthy ICR mice.

liver into the gastrointestinal tract, while less charged moieties (−17.6 mV) remain sequestered within the liver.[14] Therefore, these results demonstrate that the excretion of MSNs is dependent on the shape and surface modification.

To obtain definite evidence of MSN excretion *in vivo*, the urine and fecal samples at 24 h postadministration were investigated by TEM and EDX analysis. As shown in Supporting Information, Figures S15 and S16, we clearly observed the presence of MSNs in urine and fecal samples, which was further confirmed by EDX analysis. Previous studies also found that silica NPs larger than 100 nm can be rapidly excreted from urine.[37,40] However, these studies did not show the intact evidence of NPs during urine excretion, so it is also unknown whether these NPs were excreted as intact modalities or degradation products. He *et al.* directly observed fluorescent silica NPs with diameters of 45 nm in urine by TEM.[16] On the basis of previous knowledge, large NPs, like the NSR and NLR (over

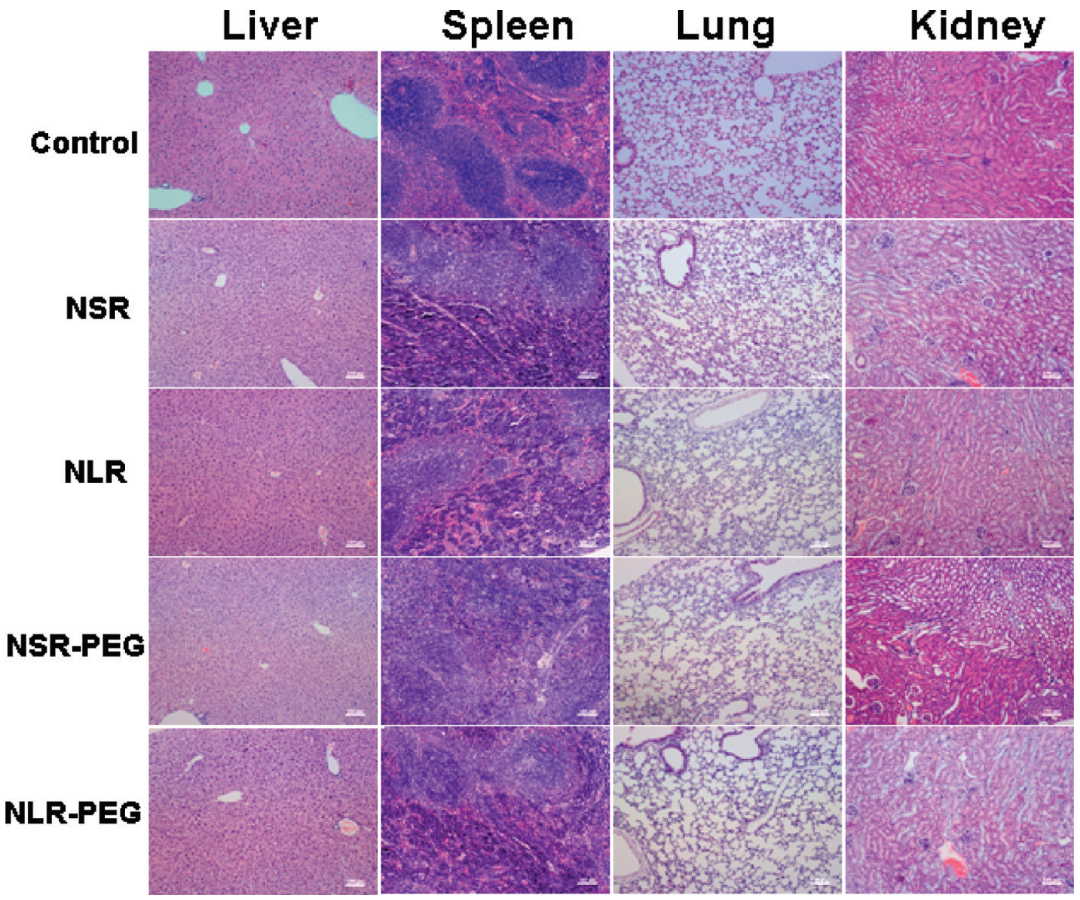

Figure 7. Effect of different shaped and PEGylated MSNs on histopathology of the liver, spleen, lung and kidney at 7 d after intravenous injection.

100 nm) used in our studies, have a hard time passing through glomerular filtration and further reach the urinary bladder. We herein show the intact excretion evidence of large sized MSNs in urine and feces, but the excreted mechanism is not clear and needs to be further studied.

Biocompatibility of Different Shaped and PEGylated MSNs *in Vivo*. When NPs are intravenously administered, the first physiological system they interact with is the blood and blood components. Then NPs would be cleared by immune cells, leave away from the bloodstream, and then reach the target organ. It is important to measure whether NPs themselves or their constituent materials would induce toxicity in the blood and organs.[41]

Immune cell uptake may cause NPs to be routed away from the site of its intended application and thus greatly reduce the number of NPs available at the target site. Therefore, understanding NP hematocompatibility is an important step during the initial characterization of nanomaterials. To study the effect of different shaped and PEGylated MSNs on blood, hematology and serum biochemical indicators were measured at 24 h and 18 d after administration of the particles. Representative hematology markers were analyzed, including red blood cell count (RBC), hemoglobin (HGB), hematocrit (HCT), mean corpuscular volume (MCV), mean corpuscular hemoglobin (MCH), mean corpuscular hemoglobin concentration (MCHC), platelet count (PLT), and white blood cell count (WBC). All hematology marker values were mostly within normal ranges and did not indicate a trend of toxicity associated with shape and PEGylation of particles (Figure 6A,B, Supporting Information, Table S1). These results indicate both MSNs and PEGylated MSNs have excellent biocompatibility in hematology.

To investigate the effect of different shaped and PEGylated MSNs on target organs, representative serum biochemical indicators, such as alanine aminotransferase (ALT), aspartate aminotransferase (AST), total bilirubin (TBIL), alkaline phosphatase (ALP), creatinine (CREA) and blood urea nitrogen (BUN), were quantified 24 h and 18 d after the administration of particles (Figure 6C,D, Supporting Information, Table S1). ALT and AST are commonly used as biochemical markers for liver function.[42] The activity of ALT and AST of naked and PEGylated MSNs were within the normal value, indicating that the particles did not influence liver function. However, we found the activity of TBIL, as a marker for biliary function, was changed after injection of MSNs. Moreover, the activity of CREA and BUN, indicators of glomerular filtration, were also outside the normal range. We can also find there were

mostly larger effects on TBIL, CREA, and BUN by NSRs. Combined with the result of direct detection of MSNs in urine and feces, we think that naked and PEGylated MSNs may induce the dysfunction of biliary excretion and glomerular filtration, causing the excretion of large sized particles (over 100 nm) by urine and feces.

To further investigate the toxicity of target organs, histological assessment of tissues was performed to determine whether different shaped and PEGylated MSNs would cause tissue damage, inflammation, or lesions at 18 d after the injection. Four representative organs including liver, spleen, lung, and kidney were fixed, stained, and analyzed. As shown in Figure 7, there were no apparent histopathological abnormalities or lesions for the groups treated with MSNs compared with that for the control group.

From the above results, different shaped MSNs have different effects on biochemical markers, but the value of hematologic markers were generally within normal ranges. We found that all four kinds of the designed MSNs did not significantly induce serious toxicity in hematology and organs except for the potential dysfunction of biliary excretion and glomerular filtration. In our previous report, we also showed no or low toxicity of MSNs when intravenously injected at single doses or repeated administrations, even at particle concentrations up to 1000 mg/kg mice.[38] Combined with *in vitro* and *in vivo* studies reported in recent years,[40,42−47] it can be summarized that MSNs have good biocompatibility. Possible reasons can be explained by the special meso-structural properties of MSNs, as demonstrated by Lin and co-workers.[44] In this study, shape effect of MSNs on *in vivo* toxicity were not observed. The reason is that MSNs have good biocompatibility, so it is difficult to compare the MSN shape effects on *in vivo* toxicity.

CONCLUSION

In this study, the fabrication of MSNs and MSN−FITC can be controlled by varying the concentration of reaction reagents, especially for the control of a series of shapes. We show *in vivo* biodistribution, clearance, and biocompatibility effects from MSN shape and PEG modification. These findings provide strong evidence that nanostructures not only actively interact with cells, but also engage in and mediate *in vivo* behaviors. Thus, the interplay between biological effects and particle shape will undoubtedly be an important aspect in investigating numerous areas of interest, including design of targeting strategies for therapeutic applications and the environmental fate of NPs. Given this result, it is necessary that shape effect studies should be expanded to a wide range of NPs to characterize NP toxicity *in vivo* using standard clinical procedures.

EXPERIMENTAL METHOD

Materials. Cetyltrimethylammonium bromide (CTAB), tetraethyl orthosilicate (TEOS), aqueous ammonia, 3-aminopropyltriethoxysilane (APTES), dimethylformamide (DMF), and sucrose were obtained from Beijing Chemical Reagents Company (China). Heparin, fluorescein isothiocyanate (FITC), hematoxylin and eosin were purchased from Sigma.

Fabrication and Characterization of MSN−FITC. Different shaped MSN−FITC particles were synthesized according to the two-step preparation previously reported.[48] First, 3-aminopropyl triethoxysilane−fluorescein isothiocyanate (APTES−FITC) was formed by stirring fluorescein isothiocyanate (FITC) in ethanolic APTES solution (the amount of FITC was 9 mol % of APTES) in the dark for 24 h. Separately, CTAB was dissolved in 70 mL of H_2O, and $NH_3 \cdot H_2O$ (28%∼30%) was added with magnetic stirring for 1 h. Two-third of TEOS was then added with vigorous stirring for 1 h at room temperature. APTES−FITC was added, and the additional one-third of TEOS was added with vigorous stirring for 4 h. The shape and size of MSN−FITCs were controlled by changing the concentration of reaction reagents. Different shaped MSN−FITCs were fabricated and the particle ARs were varied from ∼1 to ∼8 when the CTAB concentration increased from 2.94 to 19.6 mM. The concentration of aqueous ammonia played an important role in the diameter of MSN−FITC. For example, ∼70 nm MSN−FITC with ARs of ∼1.5 were produced with reactant concentrations of 5.9 mM CTAB, 171 mM $NH_3 \cdot H_2O$, and 41 mM TEOS, while ∼160 nm MSN−FITC with ARs of ∼1.5 were obtained by increasing the ammonia concentration to 256 mM. Different shaped MSN−FITC were collected by centrifugation at 15 000 *g* for 20 min and then washed and redispersed several times with deionized water and ethanol. Surfactant templates were removed by extraction in acidic ethanol (1 mL of concentrated HCl in 50 mL of ethanol) for 24 h. The particles were collected by centrifugation and then washed and redispersed several times with deionized water.

Morphology and structure of the resulting MSN−FITC were observed with a JEM-2100 transmission electron microscope (TEM). The UV−visible spectra were recorded at room temperature on a Japan JASCO V-570 UV−visible spectrometer. The fluorescent spectra of MSN−FITC were acquired with a VARIAN fluorescence spectrophotometer.

PEG Modification of MSN−FITC. Particle surfaces were first functionalized with primary amines, using 3-aminopropyltriethoxysilane (APTES) to attach alkoxy silane groups to surface hydroxyls. These amine groups were then attached with activated mPEG-SC (mPEG-succinimidyl carbonate, MW 5000) molecules. A 50 mg portion of the MSN−FITC was dispersed in 20 mL of anhydrous ethanol. A solution of 5 μL of APTES diluted in 200 μL of ethanol was added to the particle suspensions and stirred at room temperature for 20 h. The modified particles were collected by centrifugation. After washing three times, the modified particles were resuspended in 3 mL of Tris-Cl buffer (pH 8.6). Then 5 mg of mPEG-SC was added. The suspension was stirred for 8 h, and the PEG modified particles (MSN−FITC-PEG) were collected by centrifugation.

Animal Intravenous Injection and Sample Collection. Mice of 6−8 weeks old weighing 25−30 g were used for the study. For the imaging of NPs in organs, five groups were separated into cages (n = 6), control, FITC labeled short rod NPs (NSR−FITC), FITC labeled long rod NPs (NLR−FITC), PEG modified NSR−FITC (NSR−FITC−PEG), and PEG modified NLR−FITC (NLR−FITC−PEG), respectively. For quantitative analysis of silicon content by inductively coupled plasma atomic emission spectroscopy (ICP−OES), five groups were also separated into cages (n = 6), control, NSR−FITC, NLR−FITC, NSR−FITC−PEG, NLR−FITC−PEG, respectively. NP suspensions (in 5 wt % glucose injection) were injected intravenously at a dose of 20 mg/kg. After 24 h and 18 d postinjection, blood was drawn for hematology and serum biochemistry analysis using a standard vein blood collection technique. Analysis of standard hematology and serum

biochemistry was performed by the Clinical Laboratory of Capital Medical University (Beijing, China). Mice were sacrificed 2 h, 24 h and 7 d after administration and the following organs were collected: liver, kidneys, spleen, lungs, brain, and limb lymph nodes. The organs were used to analyze Si content and histopathology. To measure the excretion of MSNs from urine and feces, special single-mouse metabolic cages were used. Urine and feces were collected into separate collection tubes at different time points after the injections. The collected urine and feces were also analyzed by ICP-OES for silicon element. TEM image and energy-dispersed X-ray spectrum (EDS) analysis were also used for qualitative observation of urine and feces. The collected urine and fecal samples were respectively centrifuged. The precipitates were incubated with 1 M HCl solution for 1 h and centrifuged again. The pretreated precipitates were washed three times with water, suspended in water, and observed by TEM and analyzed by EDS (JEOL JEM 2010F).

Histological Analysis. To detect the biodistribution of MSN–FITC, half the tissue samples were snap-frozen and 5 μm cryosections were prepared to check the biodistribution of fluorescence MSNs by fluorescence microscopy. Specifically, the histology sections were stained with 4′,6′-diamidino-2-phenylindole (DAPI) and observed under a fluorescence microscope.

For histological studies, the other half of the tissues were fixed in 10% neutral buffered formalin. Then they were embedded in paraffin, and approximately 4 μm thick sections were cut and stained with hematoxylin and eosin (H&E). The histological sections were observed under an optical microscope.

Quantitative Analysis of Silicon Contents by ICP–OES. Silicon contents of blood samples, organs, urine, and feces were determined by ICP–OES against common standards ((ICP–OES, Varian Vista-MPX, US, Testing Center of Tsinghua University, Beijing, China).

Statistical Analysis. The level of significance in all statistical analyses was set at a probability of $p < 0.05$. Data are presented as mean $\pm$ SD. Analysis of variance (ANOVA) and *t* tests were used to analyze the data.

Acknowledgment. The authors acknowledge financial support from the National Natural Science Foundation (No. 30900349, 60736001 and 30800258). X. Huang thanks Swierczewska Maggie (National Institute of Biomedical Imaging and Bioengineering, NIH) for the proof editing of this manuscript and Dr. Xiaoyuan Chen (National Institute of Biomedical Imaging and Bioengineering, NIH) for his support.

Supporting Information Available: Fluorescent properties and zeta potential of MSNs, serum stability of MSN, confocal microscopy images of organs 2 h and 7 d postadministration, ICP–OES data showing biodistribution in organs, TEM and EDS of MSNs in urine and feces samples, and effect of MSN on hematology and serum biochemistry. This material is available free of charge *via* the Internet at http://pubs.acs.org.

REFERENCES AND NOTES

1. Dobrovolskaia, M. A.; Aggarwal, P.; Hall, J. B.; McNeil, S. E. Preclinical Studies to Understand Nanoparticle Interaction with the Immune System and Its Potential Effects on Nanoparticle Biodistribution. *Mol. Pharmaceutics* **2008**, *5*, 487–495.
2. Liu, H. Y.; Chen, D.; Li, L. L.; Liu, T. L.; Tan, L. F.; Wu, X. L.; Tang, F. Q. Multifunctional Gold Nanoshells on Silica Nanorattles: A Platform for the Combination of Photothermal Therapy and Chemotherapy with Low Systemic Toxicity. *Angew. Chem., Int. Ed.* **2011**, *50*, 891–895.
3. Li, L. L.; Tang, F. Q.; Liu, H. Y.; Liu, T. L.; Hao, N. J.; Chen, D.; Teng, X.; He, J. Q. *In Vivo* Delivery of Silica Nanorattle Encapsulated Docetaxel for Liver Cancer Therapy with Low Toxicity and High Efficacy. *ACS Nano* **2010**, *4*, 6874–6882.
4. Vallhov, H.; Gabrielsson, S.; Stromme, M.; Scheynius, A.; Garcia-Bennett, A. E. Mesoporous Silica Particles Induce Size Dependent Effects on Human Dendritic Cells. *Nano Lett.* **2007**, *7*, 3576–3582.
5. Jiang, W.; Kim, B. Y. S.; Rutka, J. T.; Chan, W. C. W. Nanoparticle-Mediated Cellular Response Is Size-Dependent. *Nat. Nanotechnol.* **2008**, *3*, 145–150.
6. Chithrani, B. D.; Ghazani, A. A.; Chan, W. C. Determining the Size and Shape Dependence of Gold Nanoparticle Uptake into Mammalian cells. *Nano Lett.* **2006**, *6*, 662–668.
7. Chung, T. H.; Wu, S. H.; Yao, M.; Lu, C. W.; Lin, Y. S.; Hung, Y.; Mou, C. Y.; Chen, Y. C.; Huang, D. M. The Effect of Surface Charge on the Uptake and Biological Function of Mesoporous Silica Nanoparticles 3T3-L1 Cells and Human Mesenchymal Stem Cells. *Biomaterials* **2007**, *28*, 2959–2966.
8. Pan, Y.; Neuss, S.; Leifert, A.; Fischler, M.; Wen, F.; Simon, U.; Schmid, G.; Brandau, W.; Jahnen-Dechent, W. Size-Dependent Cytotoxicity of Gold Nanoparticles. *Small* **2007**, *3*, 1941–1949.
9. Hu, Y.; Xie, J. W.; Tong, Y. W.; Wang, C. H. Effect of PEG Conformation and Particle Size on the Cellular Uptake Efficiency of Nanoparticles with the HepG2 Cells. *J. Controlled Release* **2007**, *118*, 7–17.
10. Faure, A. C.; Dufort, S.; Josserand, V.; Perriat, P.; Coll, J. L.; Roux, S.; Tillement, O. Control of the *in Vivo* Biodistribution of Hybrid Nanoparticles with Different Poly(ethylene glycol) Coatings. *Small* **2009**, *5*, 2565–2575.
11. Lin, Y. S.; Haynes, C. L. Impacts of Mesoporous Silica Nanoparticle Size, Pore Ordering, and Pore Integrity on Hemolytic Activity. *J. Am. Chem. Soc.* **2010**, *132*, 4834–4842.
12. Choi, H. S.; Ipe, B. I.; Misra, P.; Lee, J. H.; Bawendi, M. G.; Frangioni, J. V. Tissue- and Organ-Selective Biodistribution of NIR Fluorescent Quantum Dots. *Nano Lett.* **2009**, *9*, 2354–2359.
13. Schipper, M. L.; Iyer, G.; Koh, A. L.; Cheng, Z.; Ebenstein, Y.; Aharoni, A.; Keren, S.; Bentolila, L. A.; Li, J. Q.; Rao, J. H.; *et al.* Particle Size, Surface Coating, and PEGylation Influence the Biodistribution of Quantum Dots in Living Mice. *Small* **2009**, *5*, 126–134.
14. Souris, J. S.; Lee, C. H.; Cheng, S. H.; Chen, C. T.; Yang, C. S.; Ho, J. A.; Mou, C. Y.; Lo, L. W. Surface Charge-Mediated Rapid Hepatobiliary Excretion of Mesoporous Silica Nanoparticles. *Biomaterials* **2010**, *31*, 5564–5574.
15. De Jong, W. H.; Hagens, W. I.; Krystek, P.; Burger, M. C.; Sips, A. J.; Geertsma, R. E. Particle Size-Dependent Organ Distribution of Gold Nanoparticles after Intravenous Administration. *Biomaterials* **2008**, *29*, 1912–1919.
16. He, X. X.; Nie, H. L.; Wang, K. M.; Tan, W. H.; Wu, X.; Zhang, P. F. *In Vivo* Study of Biodistribution and Urinary Excretion of Surface-Modified Silica Nanoparticles. *Anal. Chem.* **2008**, *80*, 9597–9603.
17. Geng, Y.; Dalhaimer, P.; Cai, S. S.; Tsai, R.; Tewari, M.; Minko, T.; Discher, D. E. Shape Effects of Filaments *versus* Spherical Particles in Flow and Drug Delivery. *Nat. Nanotechnol.* **2007**, *2*, 249–255.
18. Gratton, S. E.; Ropp, P. A.; Pohlhaus, P. D.; Luft, J. C.; Madden, V. J.; Napier, M. E.; DeSimone, J. M. The Effect of Particle Design on Cellular Internalization Pathways. *Proc. Natl. Acad. Sci. U.S.A.* **2008**, *105*, 11613–11618.
19. Zhang, K.; Fang, H. F.; Chen, Z. Y.; Taylor, J. S. A.; Wooley, K. L. Shape Effects of Nanoparticles Conjugated with Cell-Penetrating Peptides (HIV Tat PTD) on CHO Cell Uptake. *Bioconjugate Chem.* **2008**, *19*, 1880–1887.
20. Geng, Y.; Dalhaimer, P.; Cai, S.; Tsai, R.; Tewari, M.; Minko, T.; Discher, D. E. Shape Effects of Filaments *versus* Spherical Particles in Flow and Drug Delivery. *Nat. Nanotechnol.* **2007**, *2*, 249–255.
21. Champion, J. A.; Katare, Y. K.; Mitragotri, S. Particle Shape: A New Design Parameter for Micro- and Nanoscale Drug Delivery Carriers. *J. Controlled Release* **2007**, *121*, 3–9.
22. Giri, S.; Trewyn, B. G.; Lin, V. S. Y. Mesoporous Silica Nanomaterial-Based Biotechnological and Biomedical Delivery Systems. *Nanomedicine* **2007**, *2*, 99–111.
23. Vallet-Regi, M.; Balas, F.; Arcos, D. Mesoporous Materials for Drug Delivery. *Angew. Chem., Int. Ed.* **2007**, *46*, 7548–7558.
24. Slowing, I. I.; Trewyn, B. G.; Giri, S.; Lin, V. S. Y. Mesoporous Silica Nanoparticles for Drug Delivery and Biosensing Applications. *Adv. Funct. Mater.* **2007**, *17*, 1225–1236.

25. Tsai, C. P.; Hung, Y.; Chou, Y. H.; Huang, D. M.; Hsiao, J. K.; Chang, C.; Chen, Y. C.; Mou, C. Y. High-Contrast Paramagnetic Fluorescent Mesoporous Silica Nanorods as a Multifunctional Cell-Imaging Probe. *Small* **2008**, *4*, 186–191.
26. Huang, X. L.; Teng, X.; Chen, D.; Tang, F. Q.; He, J. Q. The Effect of the Shape of Mesoporous Silica Nanoparticles on Cellular Uptake and Cell Function. *Biomaterials* **2010**, *31*, 438–448.
27. Ow, H.; Larson, D. R.; Srivastava, M.; Baird, B. A.; Webb, W. W.; Wiesner, U. Bright and Stable Core-Shell Fluorescent Silica Nanoparticles. *Nano Lett.* **2005**, *5*, 113–117.
28. Wang, L.; Tan, W. H. Multicolor FRET Silica Nanoparticles by Single Wavelength Excitation. *Nano Lett.* **2006**, *6*, 84–88.
29. Burns, A.; Ow, H.; Wiesner, U. Fluorescent Core−Shell Silica Nanoparticles: Towards "Lab on a Particle" Architectures for Nanobiotechnology. *Chem. Soc. Rev.* **2006**, *35*, 1028–1042.
30. Li, S. D.; Huang, L. Pharmacokinetics and Biodistribution of Nanoparticles. *Mol. Pharm.* **2008**, *5*, 496–504.
31. Pappalardo, M.; Milardi, D.; Grasso, D.; La Rosa, C. Phase Behaviour of Polymer-Grafted DPPC Membranes for Drug Delivery Systems Design. *J. Therm. Anal. Calorim.* **2005**, *80*, 413–418.
32. Sofia, S.; Premnath, V.; Merrill, E. Poly(Ethylene Oxide) Grafted to Silicon Surfaces: Grafting Density and Protein Adsorption. *Macromolecules* **1998**, *31*, 5059–5070.
33. Inoue, Y.; Kiryu, S.; Watanabe, M.; Oyaizu, N.; Ohtomo, K. Fluorescence Lymph Node Mapping in Living Mice Using Quantum Dots and a Compression Technique. *J. Fluoresc.* **2010**, *20*, 599–606.
34. Ku, S. T.; Yan, F.; Wang, Y.; Sun, Y.; Yang, N.; Ye, L. The Blood-Brain Barrier Penetration and Distribution of PEGylated Fluorescein-Doped Magnetic Silica Nanoparticles in Rat Brain. *Biochem. Biophys. Res. Commun.* **2010**, *394*, 871–876.
35. Cho, W. S.; Cho, M.; Jeong, J.; Choi, M.; Han, B. S.; Shin, H. S.; Hong, J.; Chung, B. H.; Jeong, J.; Cho, M. H. Size-Dependent Tissue Kinetics of PEG-Coated Gold Nanoparticles. *Toxicol. Appl. Pharmacol.* **2010**, *245*, 116–123.
36. Calvo, P.; Gouritin, B.; Chacun, H.; Desmaele, D.; D'Angelo, J.; Noel, J. P.; Georgin, D.; Fattal, E.; Andreux, J. P.; Couvreur, P. Long-Circulating PEGylated Polycyanoacrylate Nanoparticles as New Drug Carrier for Brain Delivery. *Pharm. Res.* **2001**, *18*, 1157–1166.
37. He, Q. J.; Zhang, Z. W.; Gao, F.; Li, Y. P.; Shi, J. L. *In Vivo* Biodistribution and Urinary Excretion of Mesoporous Silica Nanoparticles: Effects of Particle Size and PEGylation. *Small* **2011**, *7*, 271–280.
38. Liu, T. L.; Li, L. L.; Teng, X.; Huang, X. L.; Liu, H. Y.; Chen, D.; Ren, J.; He, J. Q.; Tang, F. Q. Single and Repeated Dose Toxicity of Mesoporous Hollow Silica Nanoparticles in Intravenously Exposed Mice. *Biomaterials* **2011**, *32*, 1657–1668.
39. Liu, Z.; Davis, C.; Cai, W. B.; He, L. N.; Chen, X. Y.; Dai, H. J. Circulation and Long-Term Fate of Functionalized, Biocompatible Single-Walled Carbon Nanotubes in Mice Probed by Raman Spectroscopy. *Proc. Natl. Acad. Sci. U. S.A.* **2008**, *105*, 1410–1415.
40. Lu, J.; Liong, M.; Li, Z.; Zink, J. I.; Tamanoi, F. Biocompatibility, Biodistribution, and Drug-Delivery Efficiency of Mesoporous Silica Nanoparticles for Cancer Therapy in Animals. *Small* **2010**, *6*, 1794–1805.
41. Hauck, T. S.; Anderson, R. E.; Fischer, H. C.; Newbigging, S.; Chan, W. C. *In Vivo* Quantum-Dot Toxicity Assessment. *Small* **2010**, *6*, 138–144.
42. Jain, T. K.; Reddy, M. K.; Morales, M. A.; Leslie-Pelecky, D. L.; Labhasetwar, V. Biodistribution, Clearance, and Biocompatibility of Iron Oxide Magnetic Nanoparticles in Rats. *Mol. Pharm.* **2008**, *5*, 316–327.
43. Lin, Y. S.; Haynes, C. L. Impacts of Mesoporous Silica Nanoparticle Size, Pore Ordering, and Pore Integrity on Hemolytic Activity. *J. Am. Chem. Soc.* **2010**, *132*, 4834–4842.
44. Slowing, I. I.; Wu, C. W.; Vivero-Escoto, J. L.; Lin, V. S. Y. Mesoporous Silica Nanoparticles for Reducing Hemolytic Activity towards Mammalian Red Blood Cells. *Small* **2009**, *5*, 57–62.
45. Slowing, I. I.; Vivero-Escoto, J. L.; Wu, C. W.; Lin, V. S. Y. Mesoporous Silica Nanoparticles as Controlled Release Drug Delivery and Gene Transfection Carriers. *Adv. Drug Delivery Rev.* **2008**, *60*, 1278–1288.
46. Huang, D. M.; Chung, T. H.; Hung, Y.; Lu, F.; Wu, S. H.; Mou, C. Y.; Yao, M.; Chen, Y. C. Internalization of Mesoporous Silica Nanoparticles Induces Transient but Not Sufficient Osteogenic Signals in Human Mesenchymal Stem Cells. *Toxicol. Appl. Pharmacol.* **2008**, *231*, 208–215.
47. Vivero-Escoto, J. L.; Slowing, I. I.; Lin, V. S. Y. Tuning the Cellular Uptake and Cytotoxicity Properties of Oligonucleotide Intercalator-Functionalized Mesoporous Silica Nanoparticles with Human Cervical Cancer Cells HeLa. *Biomaterials* **2010**, *31*, 1325–1333.
48. Huang, D. M.; Hung, Y.; Ko, B. S.; Hsu, S. C.; Chen, W. H.; Chien, C. L.; Tsai, C. P.; Kuo, C. T.; Kang, J. C.; Yang, C. S.; *et al*. Highly Efficient Cellular Labeling of Mesoporous Nanoparticles in Human Mesenchymal Stem Cells: Implication for Stem Cell Tracking. *FASAB J.* **2005**, *19*, 2014–2016.